JOURNAL OF MATERIALS SCIENCE **38** (2003) 1161 – 1169

Nanocrystalline microstructures in $Fe_{93-x}Zr_7B_x$ alloys

X. Y. XIONG*, T. R. FINLAYSON†, B. C. MUDDLE
School of Physics and Materials Engineering, Monash University, Clayton 3800, Australia
E-mail: trevor.finlayson@spme.monash.edu.au

The crystallization behaviour of amorphous $Fe_{93-x}Zr_7B_x$ ($x = 3$, 6, 12 at.%) alloys, the microstructures of the primary crystallization products of stable and metastable phases and the subsequent transformations, have been studied using a combination of differential scanning calorimetry, differential thermal analysis, X-ray diffraction and transmission electron microscopy, including microdiffraction. It has been found that, for $x = 3$ and 6 at.%, the sole product of primary crystallization is the bcc α-Fe phase and the average grain sizes of the crystalline phase were 14 nm and 12 nm for the two alloys, respectively. However, when $x = 12$ at.%, primary crystallization results in more than one crystalline phase, and a metastable phase with the cubic "$Fe_{12}Si_2ZrB$" structure is the major crystallization product after the primary crystallization reaction, accompanied by the α-Fe phase. The average grain size of this metastable phase was 35 nm for the alloy heated to 883 K at 20 K/min. Isothermal heat treatments at 873 K and 973 K confirm that after being heated for 240 h, this metastable phase transforms into equilibrium phases: bcc α-Fe, hcp ZrB_2 and probably hcp Fe_2Zr. The apparent activation energies for the primary crystallization reaction during continuous heating for these three alloys are 4.4 ± 0.2 eV, 3.5 ± 0.2 eV and 6.9 ± 0.3 eV, respectively.

1. Introduction

Nanocrystalline Fe-Zr-B alloys have aroused extensive research interest on account of their high saturation magnetization and high magnetic permeability. Studies of the effects of boron on the formation of nanocrystalline structures and magnetic properties [1, 2] have shown that the addition of boron to Fe-Zr alloys improves the glass-forming ability and refines the primary bcc α-Fe grains during crystallization, leading to an increased permeability. However, when the boron content is increased to 8 at.%, the magnetic permeability is observed to decrease [2, 3]. The change in magnetic properties is presumably related to the change in microstructures of these alloys. The microstructures of such alloys during crystallization, and the effect of boron content, especially higher boron content, on the crystallization behaviour and magnetic properties, have yet to be studied in detail.

In this paper, we report studies of the crystallization behaviour of amorphous $Fe_{93-x}Zr_7B_x$ ($x = 3$, 6, 12 at.%) alloys and the changes in microstructures for these alloys during crystallization with varying boron content. The changes in magnetic properties have been reported elsewhere [4].

2. Experimental methods

The raw materials, pure iron (99.98%), zirconium (99.8%), and boron (99.9995%) were repeatedly melted in an argon arc furnace. Amorphous $Fe_{93-x}Zr_7B_x$ ($x = 3$, 6, 12 at.%) alloy ribbons, typically 20 μm thick and 1 to 2 mm wide, were produced by melt-spinning in a helium atmosphere. The amorphous nature of the ribbons was confirmed by X-ray diffractometry (XRD) and transmission electron microscopy (TEM). Differential thermal analysis (DTA) was used to trace crystallization of the amorphous alloy ribbons over a wide temperature range, and differential scanning calorimetry (DSC) was used to investigate the kinetics of crystallization. The microstructures of the crystallized alloys were examined using XRD and TEM. Samples for TEM observation were prepared by electropolishing in an electrolyte of 5% perchloric acid, 95% methanol at about -40°C, and an applied voltage in the range 14–18 V.

3. Results and discussion

3.1. Crystallization behaviour

In Fig. 1 the resulting DTA curves measured at a heating rate of 10 K/min for the three alloys are compared. It

Present address: Materials Physics Group, National Institute for Materials Science, 1-2-1 Sengen, Tsukuba 305, Japan.
† Author to whom all correspondence should be addressed.

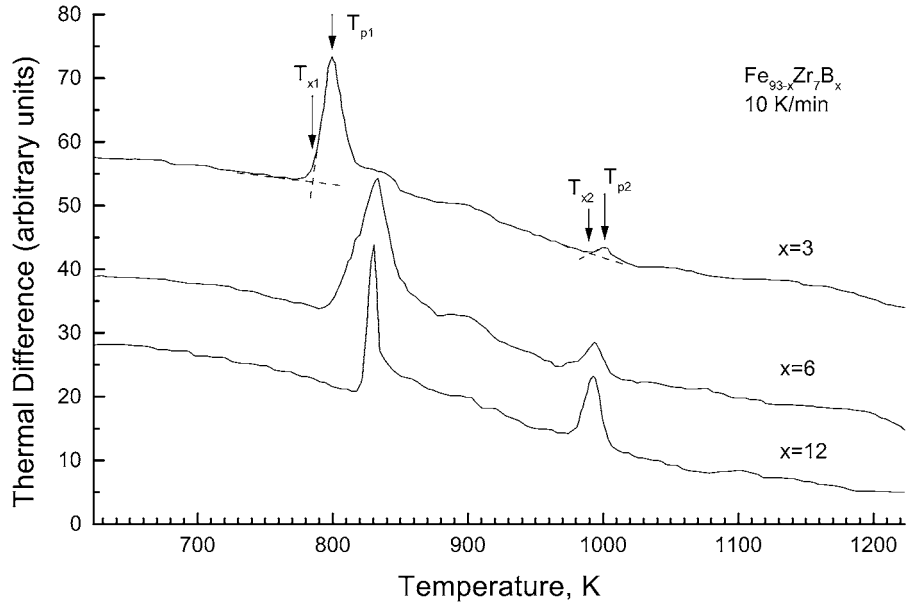

Figure 1 DTA curves for amorphous $Fe_{93-x}Zr_7B_x$ alloys.

can be seen that for each alloy there are two exothermic peaks, which is in agreement with the result reported for low-boron-content alloys [1]. These two peaks correspond to two individual crystallization reactions, suggesting that crystallization occurred in two stages. The phase transformations involved in each stage will be dealt with later. With increasing boron content, the onset temperature of the first peak, T_{x1} (as defined in Fig. 1), was displaced towards higher temperatures. For the range of the alloy compositions investigated, T_{x1} increased by a total of 36 ± 2 K, suggesting that increasing the boron content improved the thermal stability of the amorphous phase. However, the second peak temperature, T_{p2}, did not change significantly. The values of T_{x1}, T_{p1}, T_{x2} and T_{p2} are all listed in Table I.

As good soft magnetic properties are only obtained after primary crystallization [5], it is the microstructure following primary crystallization that is of most significance. The effect of boron content on the kinetics of primary crystallization has been examined using Kissinger's method [6]. DSC curves were recorded for the three alloys at various heating rates (from 5 K/min to 60 K/min). The peak temperatures and the corresponding heating rates were used to construct Kissinger plots and the resulting activation energies for the primary crystallization reactions are given in Table I.

3.2. Microstructural observations

To examine the changes in microstructure during the crystallization reaction, DSC samples were rapidly cooled from selected temperatures and then were studied using XRD and TEM.

TABLE I The onset temperatures of the first and second DTA peaks, T_{x1} and T_{x2}, the first and second DTA peak temperatures, T_{p1} and T_{p2}, and the apparent activation energies, E_a, for primary crystallization of amorphous $Fe_{93-x}Zr_7B_x$ alloys ($x = 3$, 6 and 12 at.%)

Composition	T_{x1}, (K)	T_{x2}, (K)	T_{p1}, (K)	T_{p2}, (K)	$T_{p2} - T_{p1}$, (K)	E_a, (eV)
$Fe_{90}Zr_7B_3$	786	989	803	999	196	4.4 ± 0.2
$Fe_{87}Zr_7B_6$	796	975	832	992	160	3.5 ± 0.2
$Fe_{81}Zr_7B_{12}$	822	981	830	992	162	6.9 ± 0.3

3.2.1. X-ray diffraction

Fig. 2 shows the XRD patterns for the $Fe_{90}Zr_7B_3$ samples in the as-quenched state and after being heated to the temperatures 753 K (before the primary crystallization peak), 825 K (at the primary crystallization peak), 875 K (after the primary crystallization peak) and 1003 K (after the second peak) at 20 K/min in the DSC sample holder. It can be seen that for the as-quenched sample, there is only one broad peak, with a 2θ width of about 10 degrees. For the sample heated to 753 K, a small sharp peak at $2\theta = 44.6^\circ$ is already evident, indicating partial crystallization has occurred in the alloy. For the samples heated to 825 K and 875 K, there are three diffraction peaks which are evidence of the bcc α-Fe phase. With increasing temperature, the intensities of the three α-Fe peaks increase, indicating an increase in the volume fraction of α-Fe phase present. When the temperature is increased to 1003 K, the (110) peak becomes slightly narrower than those for the samples heated to lower temperatures, suggesting that the grain size of the crystalline phase is increased, and there are two extra minor peaks emerging at the angles $2\theta = 30.3^\circ$ and 43.7°. These two peaks can be indexed for the fcc Fe_3Zr phase. In addition, the peak indexed as (110) has shifted from $2\theta = 44.6^\circ$ to 44.8°. The reason for this shift is not clear.

Using the Scherrer equation [7] and the full-widths-at-half-maximum for the (110) peaks following the 875 K and 1003 K heat treatments, the grain sizes of the bcc α-Fe phase were estimated to be 18 nm and 33 nm, respectively.

Similar results were found for the $Fe_{87}Zr_7B_6$ alloy following heat treatments at relatively comparable temperatures chosen on the basis of the DSC data, indicating that similar phase evolution processes occurred in both the $Fe_{90}Zr_7B_3$ and $Fe_{87}Zr_7B_6$ alloys, as follows:

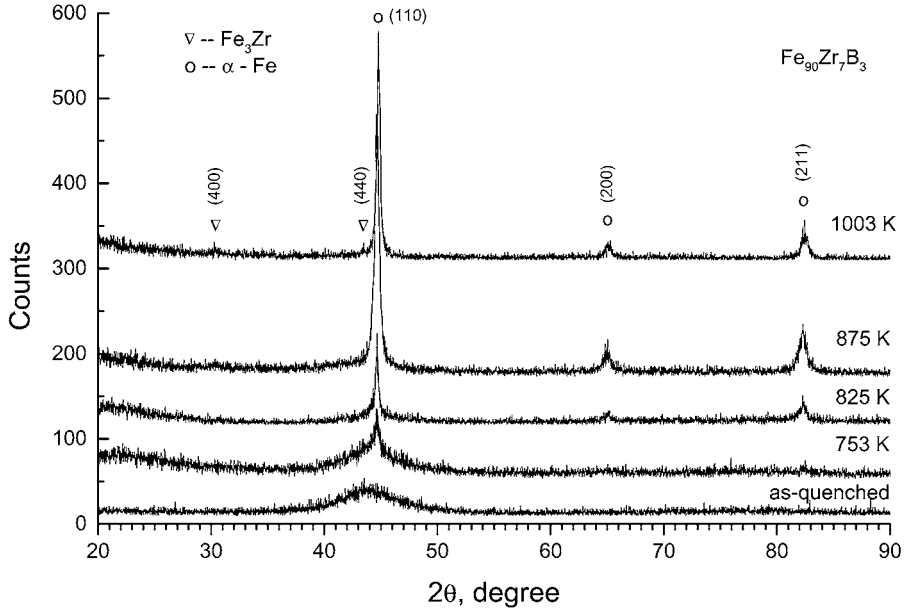

Figure 2 XRD patterns for the $Fe_{90}Zr_7B_3$ alloy samples in the as-quenched state and after being heated to temperatures of 753 K, 825 K, 875 K and 1003 K at 20 K/min.

- Amorphous → α-Fe + residual amorphous, for the primary crystallization;
- Residual amorphous → α-Fe + Fe_3Zr, for the secondary crystallization.

These results are in good agreement with previous reports of these low-boron-content alloys [3, 8].

For the $Fe_{81}Zr_7B_{12}$ alloy the crystallization reaction was distinctively different, according to the XRD measurements, although this difference was not readily evident from the DTA or DSC curves. The general form of the DTA or DSC curves was similar, with the exotherm representing primary crystallization sharper in profile than those of the alloys of lower boron contents. One as-quenched and five DSC samples for nanostructure study were prepared, representing the amorphous alloy and key temperatures on the DSC curve, and the XRD patterns of these samples are compared in Fig. 3. The final temperatures were 849 K (at the primary crystallization peak), 883 K (immediately after the primary crystallization peak), 936 K (immediately before the second peak), 953 K (immediately after the second peak) and 1003 K (far above the second peak). It can be seen in Fig. 3 that when the temperature is 849 K, crystallization is evident but the crystallization product is clearly very different from that in the alloys of lower boron contents. With increasing temperature to 883 K, additional crystalline peaks appear and these continue to increase in intensity following the 936 K heat treatment. Following heat treatment at

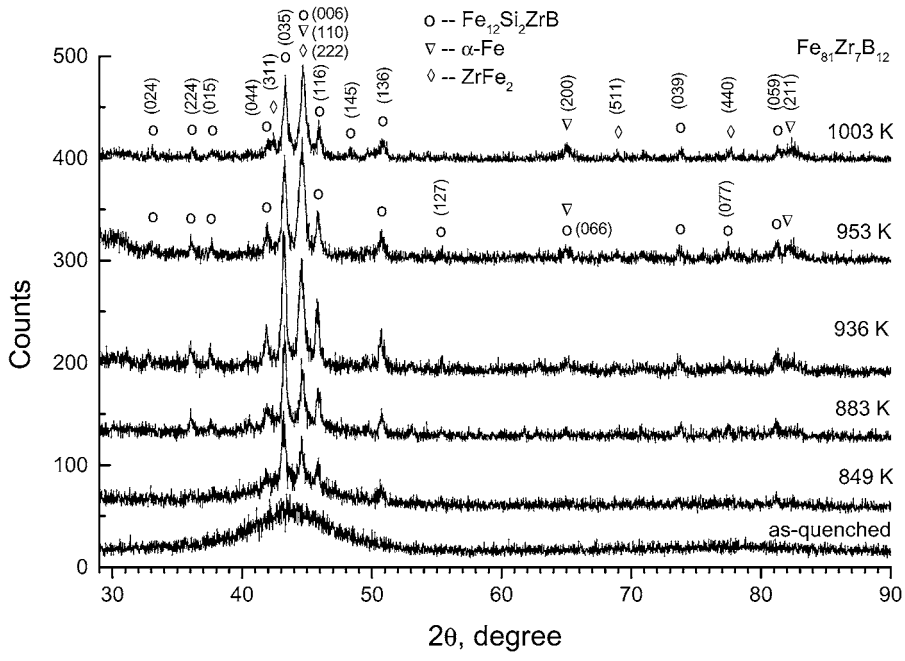

Figure 3 XRD patterns for the $Fe_{81}Zr_7B_{12}$ alloy samples in the as-quenched state and after being heated to temperatures of 849 K, 883 K, 936 K, 953 K and 1003 K at 20 K/min.

953 K, a noticeable change in the diffraction pattern has occurred, namely, a reversal in the order of the intensities of the two most intense peaks. The peak at $2\theta = 44.6^\circ$, indexed as "$Fe_{12}Si_2ZrB$" (006), changes from the next-to-strongest to the strongest peak. At this stage all peaks which one can associate with the "$Fe_{12}Si_2ZrB$" structure phase, are identified. In addition, the peaks at $2\theta = 44.6^\circ$ and 64.9° have become wider than before, on account of the initial detection of additional diffraction peaks. Following the heat treatment at 1003 K and the observation of a distinctly new peak at $2\theta = 42.5^\circ$, indexed as $ZrFe_2$ (311), other peaks index to this phase, as indicated in Fig. 3.

These results are quite different from those reported by Kopcewicz *et al.* [9], who studied the microstructure and magnetic properties of the amorphous and nanocrystalline $Fe_{81}Zr_7B_{12}$ alloy and claimed that when the alloy was heated to 823 K and 873 K, the bcc α-Fe phase was formed, accompanied by Fe_3(Zr,B) phase. However, in the present study, the XRD patterns for the samples heated to 849 K and 883 K cannot be indexed for either the α-Fe or Fe_3(Zr,B) phases or a combination of both.

As shown in Fig. 3, all diffraction peaks can be successfully indexed. For the sample heated to 883 K, all diffraction peaks observed fit the cubic phase with the "$Fe_{12}Si_2ZrB$" structure, according to the Powder Diffraction File (PDF) data available thus far [10]. When the temperature is increased to 953 K, all the diffraction peaks can be indexed by assuming a combination of the bcc α-Fe and the "$Fe_{12}Si_2ZrB$" structure phases. With increasing temperature to 1003 K, a new set of peaks with the major peak at $2\theta = 42.5^\circ$ can be indexed for the fcc $ZrFe_2$ phase.

According to the equilibrium phase diagram of Fe-Zr-B alloy system [11, 12], the bcc α-Fe and fcc $ZrFe_2$ are equilibrium phases. However, there is no indication given for the presence of a phase with the "$Fe_{12}Si_2ZrB$" structure. This suggests that such a phase must be metastable, even though it can be fairly stable at temperatures as high as 1003 K. When the temperature is increased, this phase transforms into the equilibrium phases α-Fe and $ZrFe_2$. To date, this is the first report of a metastable phase with the "$Fe_{12}Si_2ZrB$" structure to be observed in Fe-Zr-B alloys.

To understand better the crystallization kinetics and the transformation sequence in the $Fe_{81}Zr_7B_{12}$ alloy, the microstructural changes were examined during isothermal heat treatment. Alloy samples were heated rapidly to 873 K and held for 0.5 h, 2 h, 10 h, 24 h and 240 h and also to 973 K for 24 h and 240 h. The XRD patterns for the 873 K samples are shown in Fig. 4. After 0.5 h, the amorphous alloy has already partially crystallized and the observed diffraction peaks can be indexed to the metastable phase with the "$Fe_{12}Si_2ZrB$" structure. When the heating time is increased to 10 h, the diffraction pattern is almost unchanged except for the intensities of the peaks and, following a further increase to 24 h, there is evidence for small amounts of the equilibrium phases, α-Fe and cubic $ZrFe_2$. All diffraction peaks on this pattern can be indexed by employing a combination of these two minority phases and the cubic metastable phase with the "$Fe_{12}Si_2ZrB$" structure. After the alloy is held at 873 K for 24 h, the diffraction pattern most resembles one of the patterns from the continuously heated and rapidly cooled treatments, namely, the 883 K (Fig. 3). After 240 h at 873 K, the diffraction peaks of the metastable phase with the "$Fe_{12}Si_2ZrB$" structure disappear. Instead, a few additional minor peaks, plus the three major α-Fe phase peaks, are evident. All these minor peaks can be well indexed for an hexagonal Fe_2Zr phase. However, this phase is relatively uncommon, as it is the cubic Fe_2Zr phase (mentioned as $ZrFe_2$ phase earlier) that is normally formed, as shown in the equilibrium phase diagram [11, 12]. Owing to the fact that there are only two small peaks on the XRD pattern matching the hexagonal Fe_2Zr phase, it cannot yet be claimed that the additional phase is definitely the hcp Fe_2Zr.

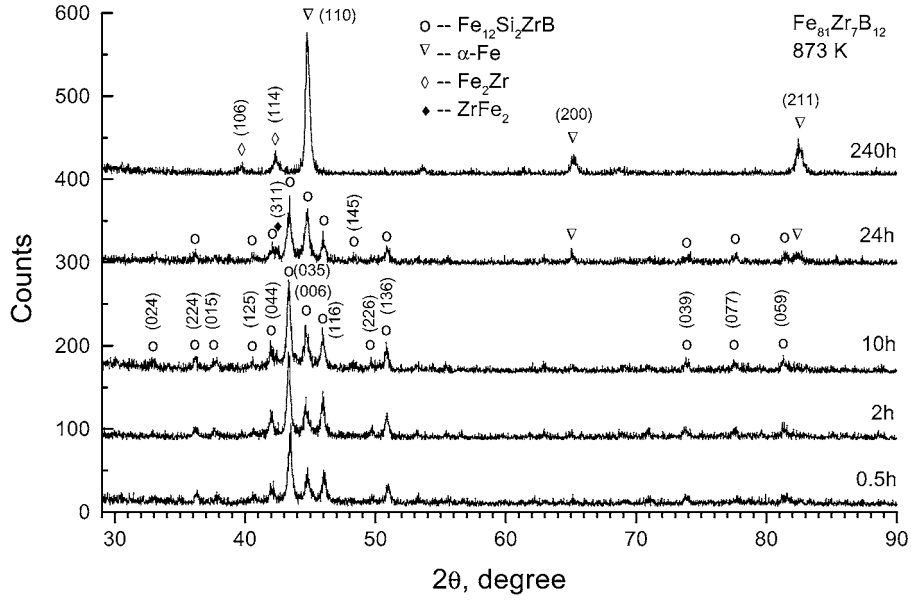

Figure 4 XRD patterns for the $Fe_{81}Zr_7B_{12}$ alloy samples heated to 873 K for 0.5 h, 2 h, 10 h, 24 h and 240 h.

At 973 K, the crystallization following 24 h is similar to that of the sample heated to 873 K for 240 h, but following 240 h at 973 K the diffraction peaks of the hcp Fe_2Zr phase disappeared. Instead, another set of minor peaks emerged. All these new minor peaks could be indexed for the hexagonal ZrB_2 phase. The phase transformation sequence occurring in the $Fe_{81}Zr_7B_{12}$ alloy at 973 K can be inferred to be as follows:

- Amorphous phase $\rightarrow$ "$Fe_{12}Si_2ZrB$" + residual amorphous phase
- "$Fe_{12}Si_2ZrB$" + residual amorphous phase $\rightarrow$ α-Fe + Fe_2Zr + residual amorphous phase
- Fe_2Zr + residual amorphous phase $\rightarrow$ α-Fe + ZrB_2.

3.2.2. Transmission electron microscopy

TEM observations were carried out on selected XRD samples. For the as-quenched alloy samples, a homogeneous structure was observed in the bright field (BF) image. The intensity distribution was quite even and no sharp contrast was observed in the field of view. A selected area diffraction (SAD) pattern only had a few concentric diffuse rings. Using a portion of the first strong diffuse ring to form a centred dark field (CDF) image, only speckled contrast was observed. No indication of the presence of crystalline structure was evident. These observations are consistent with the results reported by Zhang *et al*. [8].

This microstructure can even be observed in the $Fe_{90}Zr_7B_3$ sample heated to 753 K. A TEM BF image of this sample is shown in Fig. 5a. Within the observable area in the foil no obvious crystallization was found. The thin-foil samples remained uniform in contrast, similar to the as-quenched microstructure. However, for the specimen heated to 825 K, there was a dense distribution of crystalline grains, dispersed quite uniformly throughout an amorphous matrix. Following the complete primary crystallization reaction for the sample heated to 875 K, as shown in Fig. 5b, the SAD pattern (insert to Fig. 5b) can be fully indexed to the bcc α-Fe phase, consistent with the XRD result. The grain size of the crystalline phase was typically in the range 10–30 nm. By counting about 150 grains and using the normal distribution curve to fit the grain size data, the most probable grain size was estimated to be 14 nm for the sample heated to 875 K, which is in fairly good agreement with the value of 18 nm calculated from the X-ray line width.

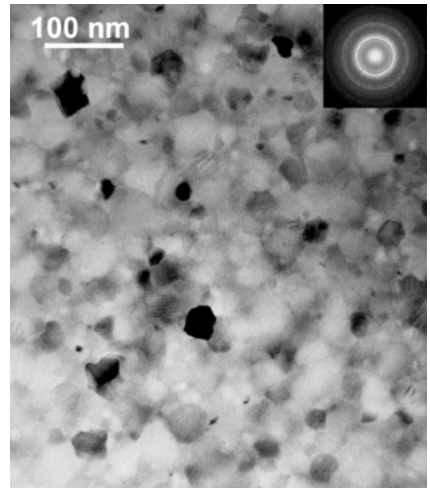

Figure 6 TEM bright field images and the corresponding SAD patterns for the $Fe_{81}Zr_7B_{12}$ nanocrystalline alloys heated to 883 K at 20 K/min.

TEM observations on the $Fe_{87}Zr_7B_6$ alloy showed similar microstructure with an average grain size of 12 nm, although many small crystals were observed to aggregate.

For the $Fe_{81}Zr_7B_{12}$ alloy, heated to 883 K, i.e. immediately after the first peak on the DSC curve, the BF image in Fig. 6 shows a fairly uniform distribution of crystalline grains. The grain size is in the range 20–60 nm, having a statistical average grain size of 35 nm. The morphology of the individual crystalline grains of this sample is similar to that of the alloys with lower boron contents, showing equiaxed, granular shape. The SAD pattern of the crystalline grains of this alloy is clearly more complex than those of the alloys with lower boron contents, which is consistent with the X-ray results.

When the temperature was increased to 936 K, the distribution of the crystalline grains remained

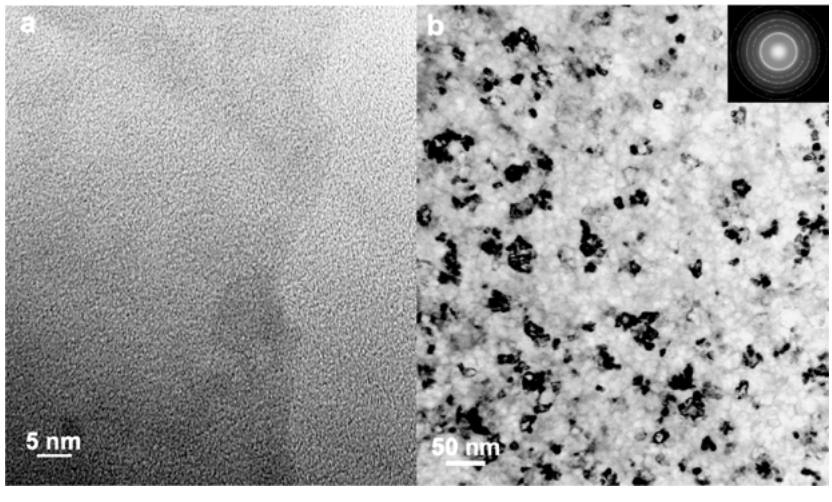

Figure 5 TEM bright field image and the corresponding SAD pattern for the $Fe_{90}Zr_7B_3$ alloy heated to (a) 753 K and (b) 875 K at 20 K/min.

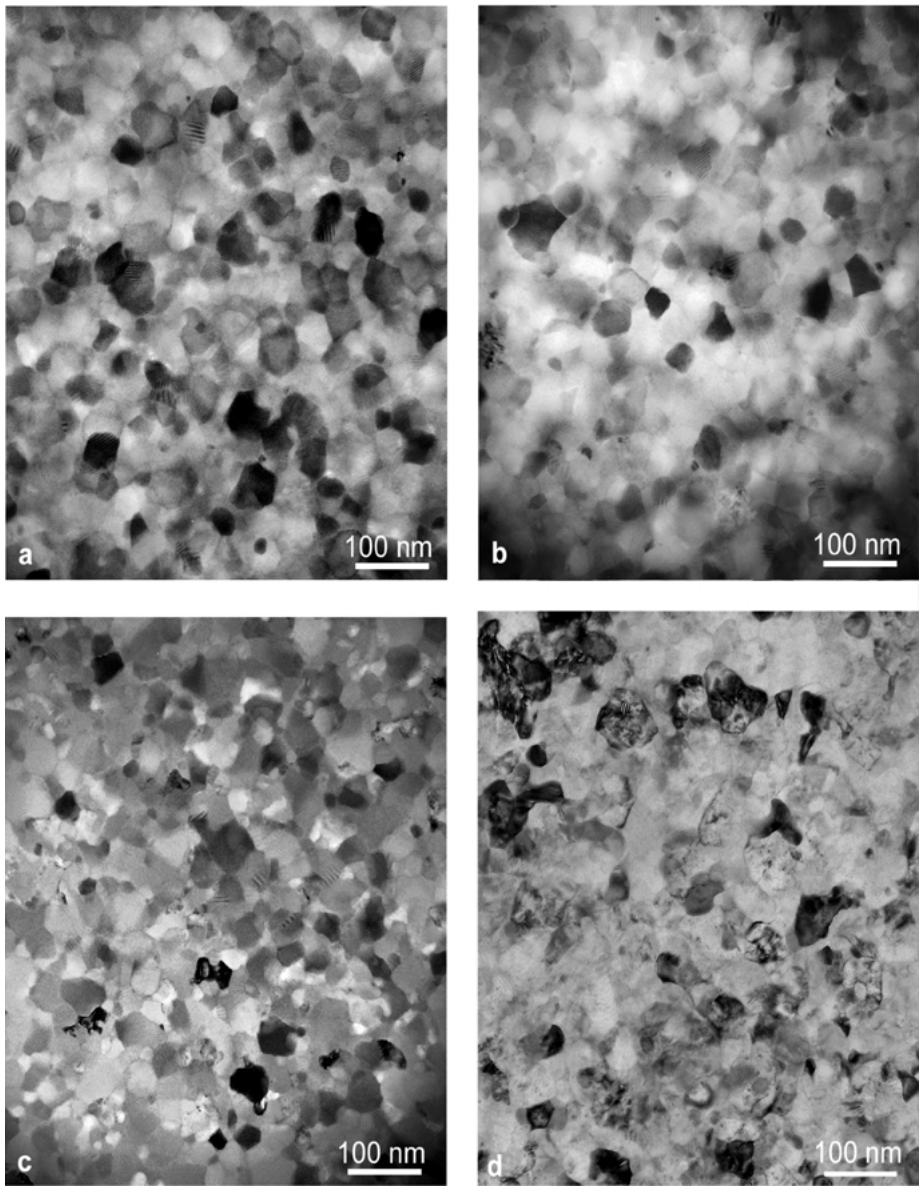

Figure 7 TEM bright field images for the $Fe_{81}Zr_7B_{12}$ alloy specimens heated to 873 K for (a) 0.5 h, (b) 2 h, (c) 24 h and (d) 240 h.

unchanged, but the grain size was increased, with an average grain size of 42 nm. On increasing temperature further to 953 K, the average grain size was roughly the same, although the SAD pattern showed that the strongest ring became sharper, i.e. the halo effect became weaker, suggesting that the volume fraction of the amorphous matrix was reduced.

Detailed TEM observations were performed on the specimens which were subjected to isothermal heating for various times. Fig. 7 shows the TEM BF images for the specimens used in Fig. 4. For the specimen heated to 873 K for 0.5 h, the crystalline phase had the form of equiaxed grains, uniformly distributed over the entire field of view. The grain size was also fairly uniform, with an average grain diameter of approximately 43 nm. With an increase in the heating time to 2 h, the grain size was no longer as uniform, with some of the grains growing at the expense of others. When the heating time was increased to 24 h, many more small grains appeared, but no distinctive feature in the shape of the grains was observed. With a further increase in the heating time to 240 h, some of the grains became very coarse, with diameters greater than 100 nm.

When the specimen was heated to 973 K, the microstructure evolved more rapidly. For the specimen heated for 24 h, the features of the BF image were similar to those of the specimen heated at 873 K for 240 h. When the heating time was increased to 240 h, the grain size became much coarser with diameters of up to 300 nm.

3.2.3. Electron microdiffraction

Since the grain size of the metastable phase was typically less than 60 nm for most of the specimens heated at 873 K for times up to 24 h (Fig. 7), microdiffraction analysis with an electron beam diameter in the range 7.5–20 nm, was adopted to confirm the identity and crystal structure of the metastable phase. Individual diffraction patterns were recorded from a series of grains. It proved very difficult to obtain multiple patterns from a single grain due to the small grain size and the overlap of neighbouring grains during tilting, and

due to sample contamination with extended exposure to a finely-focussed probe. Therefore, a compromise was made by examining the diffraction patterns statistically, i.e. observing the diffraction patterns individually from many grains (about two hundred grains were examined for each specimen in this study), and then sorting the recorded different diffraction patterns into consistent groups. Each group of diffraction patterns was indexed according to a single known crystal structure.

From all microdiffraction measurements on the specimens heated at 873 K for 0.5 h, 2 h, 10 h and 24 h, the observed diffraction patterns with high symmetry could be reduced to basically four, distinguishable, low-index patterns. These four diffraction patterns and the corresponding computer-simulated patterns are shown in Fig. 8. The computer software used for this simulation was the commercial package Desktop Microscopist—Diffraction Simulation and Analysis (Virtual Laboratories, Albuquerque, NM, USA). Two typical BF images of the particles marked with arrows, from which the microdiffraction patterns were taken, are also shown in Fig. 8a and b, for which the samples were the $Fe_{81}Zr_7B_{12}$ alloy heated at 873 K for 2 h. From these BF images, it can be seen that the features of these particles are similar to those in Fig. 7b.

The computer-simulated patterns were obtained by assuming the "$Fe_{12}Si_2ZrB$" structure [13] and replacing the silicon atoms with iron atoms, because the atomic radius of iron ($r_{Fe} = 0.126$ nm) is closer to that of silicon ($r_{Si} = 0.117$ nm) than the atomic radius of zirconium ($r_{Zr} = 0.160$ nm) [14]. It is reported [13] that the "$Fe_{12}Si_2ZrB$" structure is bcc, belonging

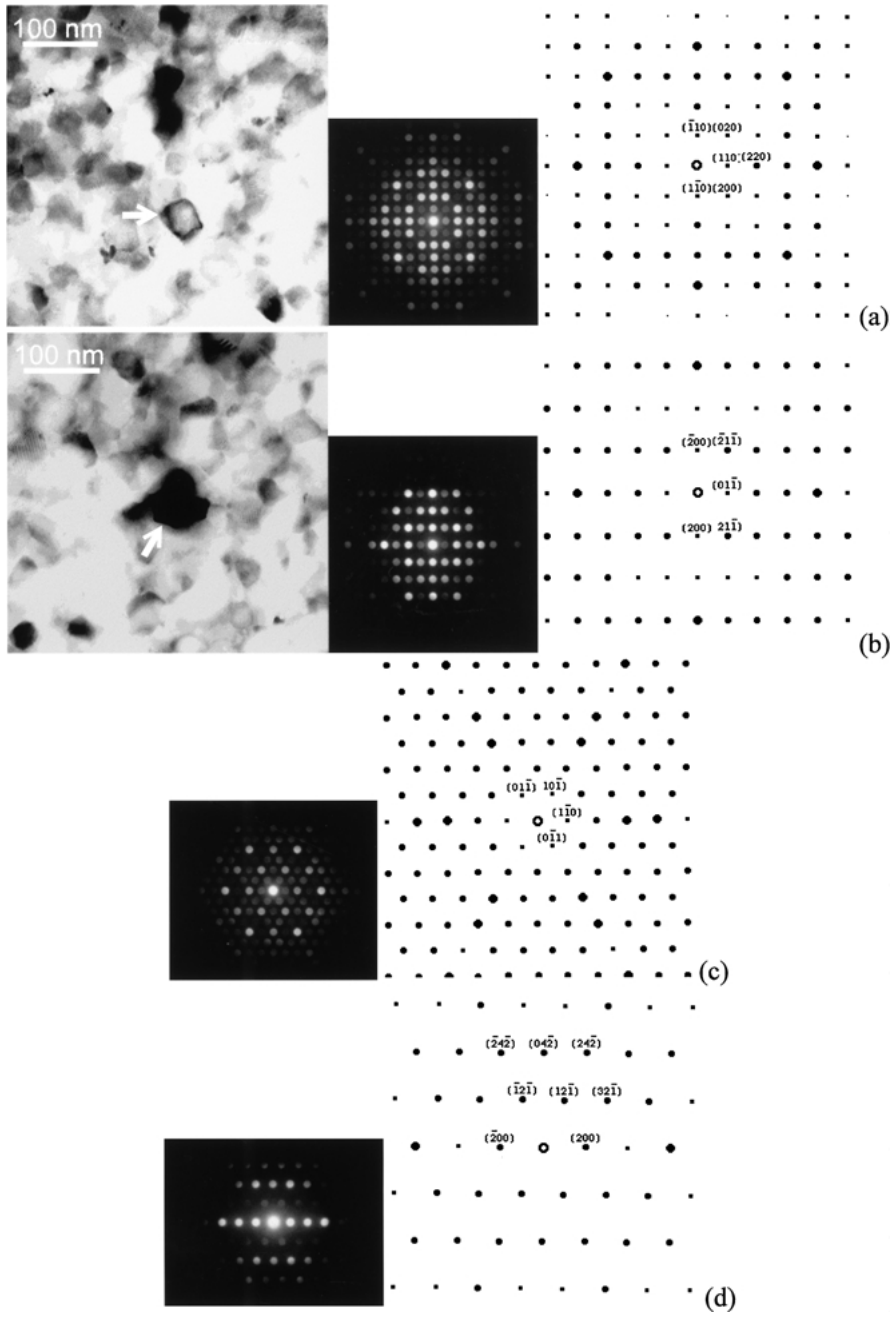

Figure 8 TEM bright field images, microdiffraction patterns and corresponding computer-simulated patterns assuming the "$Fe_{12}Si_2ZrB$" structure for the metastable phase formed in the $Fe_{81}Zr_7B_{12}$ alloy after being heated at 873 K for 0.5 h, 2 h, 10 h and 24 h. Patterns were recorded parallel to (a) [001], (b) [011], (c) [111] and (d) [012] zone axes.

to the space group $I\bar{4}3m$, with a lattice constant $a = 1.2165$ nm. The unit cell of this crystal structure contains 128 atoms.

It can be seen in Fig. 8 that the simulated patterns match the measured diffraction patterns very well. The calculated d-spacings and the angle between any two planes within the simulated patterns are in a very good agreement with those on the recorded diffraction patterns. Therefore, all diffraction patterns can be well indexed using the "$Fe_{12}Si_2ZrB$" structure. According to these indexed diffraction patterns, the lattice constant was estimated to be $a = 1.23 \pm 0.01$ nm.

It should be mentioned that the diffraction patterns were also simulated without replacing the silicon atoms with iron atoms and no differences in the intensity distribution and the geometric positions of the diffraction spots were observed between the two sets of simulated diffraction patterns, while with the silicon atoms replaced with zirconium atoms, slightly larger diffraction angles were observed in the simulated diffraction pattern.

Fig. 9 shows a lattice image including several grains of the metastable phase in the $Fe_{81}Zr_7B_{12}$ alloy heated at 873 K for 2 h. By measuring the spacing of the lattice fringes, it was found that the interplanar d-spacing was 0.87 nm, which is in a very good agreement with the d-spacing value of the closest-packed plane (110) in the bcc "$Fe_{12}Si_2ZrB$" structure ($d_{110} = 0.870$ nm).

The above electron diffraction measurements and the lattice image are quite consistent with the XRD measurements (Fig. 4), and confirm that the crystal structure of the metastable phase formed in the $Fe_{81}Zr_7B_{12}$ alloy, subjected to a heat treatment at 873 K for not longer than 24 h, has the bcc "$Fe_{12}Si_2ZrB$" structure with a lattice constant $a = 1.23$ nm.

For the specimens of the $Fe_{81}Zr_7B_{12}$ alloy heated to 873 K for 240 h and 973 K for 24 h and 240 h, the observed electron diffraction patterns with high symmetry were distinctly different from those in Fig. 8, with much larger diffraction angles. A majority of the diffraction patterns could be indexed for the cubic α-Fe phase, while other diffraction patterns could be indexed for the hexagonal phases ZrB_2 and Fe_2Zr. No diffraction patterns consistent with the fcc $ZrFe_2$ phase identified

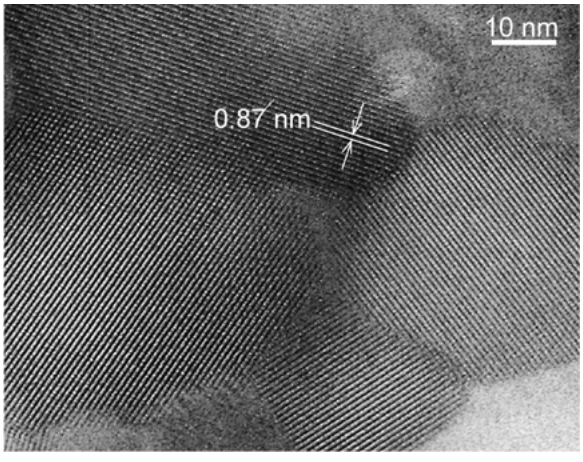

Figure 9 A lattice image of grains of the metastable phase in the $Fe_{81}Zr_7B_{12}$ alloy heated at 873 K for 2 h.

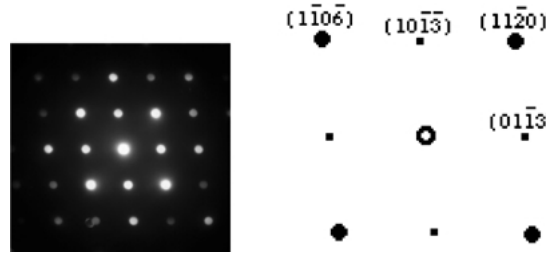

Figure 10 TEM microdiffraction pattern and corresponding computer-simulated pattern for the $Fe_{81}Zr_7B_{12}$ alloy heated to 973 K for 24 h. The simulated pattern was obtained by using the hcp Fe_2Zr structure in [$\bar{3}30\bar{1}$] zone.

in the XRD patterns in Figs 3 and 4 were detected within these electron diffraction patterns, and there was no evidence for any other phases. A TEM microdiffraction pattern taken from the sample heated at 973 K for 24 h and indexed for the hcp Fe_2Zr phase with the electron beam parallel to [$\bar{3}30\bar{1}$] zone axis, and a computer simulated pattern are shown in Fig. 10. From the indexed diffraction pattern, the lattice constants were estimated to be $a = 0.494$ nm and $c = 1.49$ nm, which are close to the reported values, $a = 0.4962$ nm and $c = 1.615$ nm [10].

All the diffraction patterns can be matched very well with the simulated patterns. The bcc α-Fe, hcp ZrB_2 and hcp Fe_2Zr phases detected by electron microdiffraction are consistent with those observed in the XRD analyses. This work also confirms that when the $Fe_{81}Zr_7B_{12}$ alloy was heated to 873 K for 240 h or 973 K for 24 h and 240 h, the metastable phase transformed into the equilibrium phases, bcc α-Fe and hcp ZrB_2, and probably hcp Fe_2Zr. Further work is needed to confirm the presence of hcp Fe_2Zr phase, rather than fcc $ZrFe_2$ phase, as given in the normal phase diagram [11].

4. Conclusions

For $Fe_{93-x}Zr_7B_x$ alloys, when the boron content is increased from 3 to 6 at.%, the crystalline phase present after the primary crystallization during continuous heating is the bcc α-Fe phase. The average grain size of the crystalline phase is 14 nm for the $Fe_{90}Zr_7B_3$ alloy heated to 875 K at 20 K/min and 12 nm for the $Fe_{87}Zr_7B_6$ alloy heated to 893 K at 20 K/min. However, when the boron content is further increased to 12 at.%, the crystalline phase formed during the primary crystallization on continuous heating is a metastable phase with the bcc "$Fe_{12}Si_2ZrB$" structure, rather than the equilibrium α-Fe phase. The average grain size of this metastable phase, obtained from the TEM observations, is 35 nm for the alloy heated to 883 K at 20 K/min. When the temperature is increased to 1003 K, the metastable phase and the residual amorphous phase start to transform into the equilibrium bcc α-Fe and fcc $ZrFe_2$ phases.

The isothermal heat treatments for the $Fe_{81}Zr_7B_{12}$ alloy at 873 K and 973 K have proved that after being heated for 240 h, the metastable phase with the bcc "$Fe_{12}Si_2ZrB$" structure transforms into equilibrium phases: bcc α-Fe, hcp ZrB_2 and probably hcp Fe_2Zr.

Acknowledgments

X. Y. Xiong acknowledges the financial support of a Monash Graduate Scholarship and an Overseas Postgraduate Research Scholarship. The authors also thank Dr. J. F. Nie for experimental assistance and Dr. K. Suzuki, formerly of the University of New South Wales, for valuable discussions.

References

1. K. SUZUKI, A. MAKINO, A. TSAI, A. INOUE and T. MASUMOTO, *Mater. Sci. and Eng.* A **179/A180** (1994) 501.
2. K. Y. KIM, T. H. NOH, I. K. KANG and T. KANG, *ibid.* **179/A180** (1994) 552.
3. K. SUZUKI, A. MAKINO, N. KATAOKA, A. INOUE and T. MASUMOTO, *Mater. Trans. JIM* **32** (1991) 93.
4. X. Y. XIONG, T. R. FINLAYSON and B. C. MUDDLE, *J. Phys. D: Appl. Phys.* **34** (2001) 2845.
5. K. SUZUKI, A. MAKINO, A. INOUE and T. MASUMOTO, *J. Appl. Phys.* **70** (1991) 6232.
6. H. E. KISSINGER, *Analyt. Chem.* **29** (1957) 1702.
7. B. D. CULLITY, "Elements of X-ray Diffraction" (Addison-Wesley Reading, MA, USA, 1959) p. 262.
8. Y. ZHANG, K. HONO, A. INOUE, A. MAKINO and T. SAKURAI, *Acta Mater.* **44** (1996) 1497.
9. M. KOPCEWICZ, A. GRABIAS, P. NOWICKI and D. L. WILLIAMSON, *J. Appl. Phys.* **79** (1996) 993.
10. PDF, 1996, *PDF-2 CD-ROM*, Version 2.14, (JCPDS—International Centre for Diffraction Data, Swarthmore, Pa, USA).
11. T. B. MASSALSKI, "Binary Alloy Phase Diagrams," 2nd ed. (ASM International, 1990) p. 1798.
12. H. OKAMOTO, "Phase Diagrams of Binary Iron Alloys" (ASM International, Materials Park, OH, 1993) p. 467.
13. Y. KHAN, *Phys. Stat. Sol. (a)* **130** (1992) K7.
14. G. H. DIEKE, in "American Institute of Physics Handbook" 2nd ed. (McGraw-Hill Book, 1963) sec. 7, p. 9.

Received 23 May
and accepted 21 November 2002